Proceedings of IMECE2005
2005 ASME International Mechanical Engineering Congress and Exposition
November 5-11, 2005, Orlando, Florida USA

IMECE2005-79102

EFFECTS OF CORNER FREQUENCY ON BANDWIDTH AND RESONANCE AMPLITUDE IN DESIGNING PZT THIN-FILM ACTUATORS: AN EXPERIMENTAL DEMONSTRATION

Chia-Che Wu
Department of Mechanical Engineering
University of Washington, Seattle, WA 98195, USA

Cheng-Chun Lee
Department of Mechanical Engineering
University of Washington, Seattle, WA 98195, USA

G. Z. Cao
Department of Material Science and Engineering
University of Washington. Seattle, WA 98195, USA

I. Y. Shen
Department of Mechanical Engineering
University of Washington, Seattle, WA 98195, USA

ABSTRACT

In the last decade, Lead Zirconate Titanate Oxide (PZT) thin-film actuators have received increasing attention because of their high frequency bandwidth, large actuation strength, fast response, and small size. The PZT film thickness is usually less than several microns as opposed to hundreds of microns for bulk PZT patches that are commercially available. As a result, PZT thin-film actuators pose unique vibration issues that do not appear in actuators with bulk PZT. Two major issues affecting actuator performance are the frequency bandwidth and the resonance amplitude. As an electromechanical device, a PZT thin-film actuator's bandwidth and resonance amplitude depend not only on the lowest natural frequency ω_n of the actuator's mechanical structure but also on the corner frequency ω_c of the actuator's *RC*-circuit. For PZT thin-film actuators, the small film thickness implies large film capacitance C and small ω_c. When the size of the actuator decreases, ω_n increases dramatically. As a result, improper design of PZT thin-film actuators could lead to $\omega_c << \omega_n$ substantially reducing the actuator bandwidth and the resonance amplitude. This paper is to demonstrate this phenomenon through calibrated experiments. In the experiments, frequency response functions of a fixed-fixed silicon beam with a 1-μm thick PZT film are measured through use of a laser Doppler vibrometer and a spectrum analyzer. The silicon beam has multiple electrodes with a wide range of resistance R and corner frequency ω_c. The experimental results confirm that the actuator bandwidth and resonance amplitude are substantially reduced when $\omega_c << \omega_n$.

INTRODUCTION

Lead Zirconate Titanate Oxide ($PbZr_{1-x}Ti_xO_3$ or PZT) thin-film actuators have received increasing attention in the last decade because of their wide applications, such as atomic force microscopes (AFM) [1,2], ultrasonic micromotors [3-6], one- or two-dimensional scanners [7-9], microswitches [10], resonators [11,12], and dual-stage actuators/sliders for next-generation computer hard disk drives [13-15]. Compared with traditional MEMS-based microactuators, PZT thin-film actuators have higher frequency bandwidth, larger actuation strength, and faster response. According to [16], there are four types of microactuators: thermal, shape-memory-alloy (SMA), electrostatic, and piezoelectric (specifically PZT). Thermal and SMA actuators have low frequency bandwidth [16] (< 1 kHz), whereas electrostatic and PZT actuators have high frequency bandwidth (> 1 kHz). Moreover, electrostatic actuators have much smaller actuation force and energy density than PZT films (3.4×10^3 J/m^3 for electrostatic actuators vs. 1.2×10^5 J/m^3 for PZT [16]).

Functionally, PZT thin-film actuators can be classified as broadband actuators and single-frequency actuators. Figure 1 shows a frequency response function (FRF) explaining the differences of these two types of actuators. Broadband actuators operate over a wide range of frequency, in which the frequency response function is approximately constant. In this frequency range, the actuator output motion is proportional to the input voltage without significant distortion. The *bandwidth* of the actuator is often defined as the frequency range in which the FRF has less than 3-db variation to minimize possible input-output distortion. Applications of broadband actuators

include AFM and microswitches for example. In this case, maximizing the bandwidth is a major design consideration because it determines how fast the tip of AFM can tap and how fast a microswitch can open and close. In contrast, single-frequency actuators operate at a single frequency, usually at a natural frequency of the actuator's mechanical structure. Example applications include resonators and scanners. In these applications, the resonance amplitude is very critical. Large resonance amplitude, for example, implies that a scanner can have a large scanning angle.

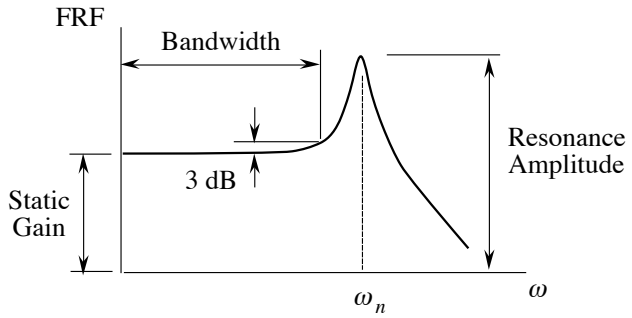

Figure 1. Frequency range of broadband and single-frequency actuators

Since PZT thin-film actuators are electromechanical devices, the actuators' performance indexes, such as bandwidth and resonance amplitude, depend not only on the actuators' mechanical structures but also on actuators' circuit design. Mechanically, the structure is a spring-mass-damper system characterized by the lowest natural frequency ω_n. Electrically, the circuit forms a low-pass *RC* filter characterized by its corner frequency ω_c. For actuators employing bulk PZT, ω_c is often a couple of orders higher than ω_n. Therefore, the actuator bandwidth and resonance amplitude are primarily dominated by the mechanical resonance frequency ω_n and the system's damping, respectively.

For PZT thin-film actuators, however, ω_c could be a couple of orders-of-magnitude less than ω_n due to the tiny thickness of PZT films. Traditional bulk PZT often appears as thin patches with thickness no less than 80 μm. In contrast, thickness of PZT thin films can vary quite substantially depending on their fabrication methods. PZT films derived from sol-gel processes—a common fabrication method for PZT films—usually have thickness less than 1 μm. As a result, the capacitance *C* of PZT thin films is significantly larger than that of bulk PZT on a per area basis, and the corner frequency ω_c of PZT thin-film actuators is reduced dramatically. As the size of PZT thin-film actuators decreases, ω_n increases significantly. Therefore, improper design of PZT thin-film actuators could lead to $\omega_c << \omega_n$ substantially reducing the actuator bandwidth and resonance amplitude. These negative effects of the corner frequency ω_c on bandwidth and resonance amplitude, however, have not been properly addressed in the literature of PZT thin-film actuators thus far [1-15].

The purpose of this paper is to demonstrate the negative effects of the corner frequency ω_c on bandwidth and resonance amplitude through calibrated experiments. For the rest of the paper, we demonstrate the negative effects of low ω_c by conducting an experiment on a matrix of fixed-fixed silicon beams with PZT thin films that offer a wide range of ω_c and ω_n. A laser Doppler vibrometer and a spectrum analyzer measure frequency response functions to determine the actuator bandwidth.

EXPERIMENTAL DEMONSTRATION

Fabrication of the specimen follows an improved sol-gel process [17] shown in Fig. 2. The silicon substrate is first oxidized in a furnace at 1045°C for 2 hours to grow a SiO_2 layer of 500 nm thick. Then a silicon nitride layer of 200 nm thick is deposited by PECVD (plasma enhanced chemical vapor deposition). The bottom electrode consists of Pt/Ti layers with thickness of 100 nm and 50 nm, respectively. The PZT film is dip-coated three times. For the first two coatings, the sintering temperature is 650°C for 15 minutes. For the third coating, the sol is diluted 50% by acetic acid and sintering temperature is 450°C for 10 minutes. The philosophy is to use the rapid thermal annealing for the first two coatings to reduce thermal stresses. For the third coating, we used diluted sol to seal possible cracks formed in the previous coatings. Finally, the top electrode consists of Au/Cr layers through evaporation. The thickness of the Au and Cr layers is 50 and 20 nm, respectively. As shown in Fig. 3, the top electrode consists of a square effective electrode, a long connecting electrode, and a rectangular soldering area. The effective electrode is the area where major actuation takes place, and it has dimensions of $4\text{ mm} \times 4\text{ mm}$. The connecting electrode has length of 32.91 mm and width of 50 μm. The soldering area has dimensions of $0.5\text{ mm} \times 1\text{ mm}$. The measured capacitance of the electrode is 40 nF. The measured resistance between the effective electrode and the soldering pad is 480 Ω.

After the PZT thin film is fabricated, the silicon wafer is diced into rectangular specimen with dimensions $74\text{ mm} \times 7.5\text{ mm} \times 0.4\text{ mm}$. The specimen is anchored at both ends via double stick tapes to simulate fixed-fixed boundary conditions. The span (i.e., distance between the anchors) *d* can vary from one specimen to another to adjust the lowest natural frequency ω_n of the specimen. Table 1 shows the test matrix. There are two parameters in the text matrix: span *d* and the electrode resistance *R*.

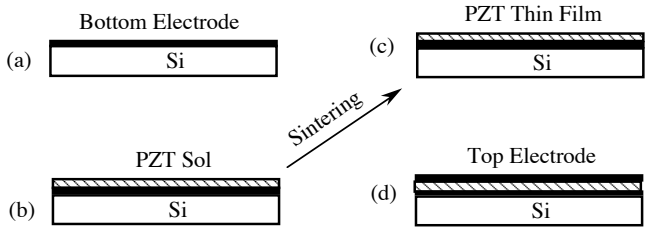

Figure 2. Sol-gel processes to make PZT thin films

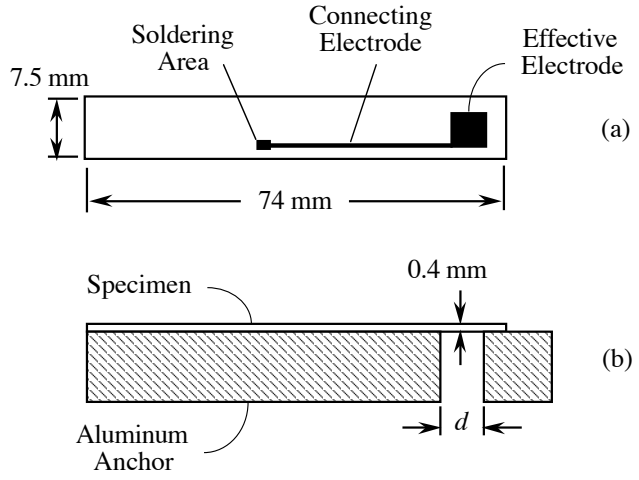

Figure 3. Specimen used in the experiments; (a) top view and (b) side view

Table 1 Test matrix in the experiments

Span	Resistance	
	Low (0.3 Ω)	High (480 Ω)
$d = 6$ mm	$\omega_c = 1.326$ MHz $\omega_n = 50.92$ kHz	$\omega_c = 8.289$ kHz $\omega_n = 50.92$ kHz
$d = 15$ mm	$\omega_c = 1.326$ MHz $\omega_n = 12.32$ kHz	$\omega_c = 8.289$ kHz $\omega_n = 12.32$ kHz

For span *d*, the test setup adopts two different spans: 6 mm and 15 mm. Based on these configurations, a finite element model is created to predict the lowest natural frequency ω_n. The finite element model consists of two portions: the silicon substrate and the anchor. The silicon substrate has thickness of 406 μm. The anchor in the form of double stick tape has a thickness of 100 μm. Table 2 lists the Young's modulus, density, and Poisson's ratio of the silicon substrate and the anchor assumed in the finite element analysis. The PZT thin film is neglected in the finite element model because of its small thickness.

Table 2 material properties used in the finite element analysis

	Thickness	Material Properties
Silicon substrate	406 μm	Young's Modulus = 110GPa Poisson Ratio = 0.278 Density = 2330 kg/m^3
Anchor via Double stick tape	100 μm	Young's Modulus = 3GPa Poisson Ratio = 0.28 Density = 1000 kg/m^3

For electrode resistance *R*, the test setup adopts two different resistance levels: high resistance 480 Ω and low resistance 0.3 Ω. For the high resistance, the lead wire is soldered to the soldering pad in Fig. 3. The resulting corner frequency is $\omega_c = 8.289$ kHz. For the low resistance, the lead wire is soldered directly onto the effective electrode shown in Fig. 5. The resulting corner frequency is $\omega_c = 1.326$ MHz. Note that the case with high resistance and short span will lead to $\omega_c << \omega_n$.

Figure 4 shows the experimental setup to measure the frequency response functions of the specimen. A spectrum analyzer generates a swept-sine signal to drive the PZT film through an amplifier. The swept-sine sweeps from 1 kHz to 100 kHZ. In the meantime, a laser Doppler vibrometer measures the vibration of the specimen at the point of largest vibration. Both the swept-sine signal and the vibrometer measurement are fed back to the spectrum analyzer to calculate the frequency response function.

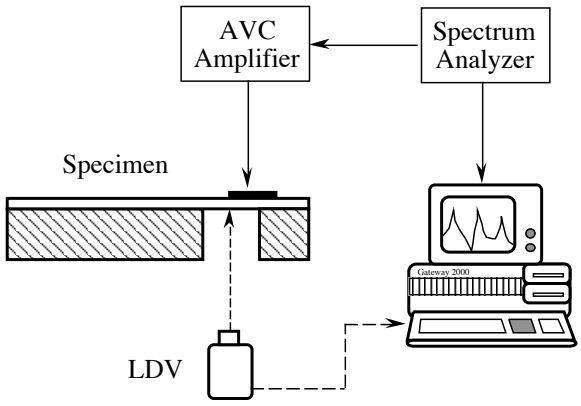

Figure 4. Experimental setup

Figure 5 compares the frequency response functions (FRF) when the span *d* is 15 mm. In Fig. 5, the thick solid line represents the FRF from the low resistance. According to Table 1, $\omega_c >> \omega_n$; therefore, the FRF starts with a constant magnitude and is followed by a resonance peak at ω_n. The 3-dB bandwidth is roughly 6.88 kHz. In contrast, the thin solid line in Fig. 5 represents the FRF corresponding to the specimen with high resistance. For the high-resistance case, ω_c is slightly smaller than ω_n. As a result, the FRF starts with a constant magnitude at low frequency, but the magnitude gradually decreases as the driving frequency increases. The 3-dB bandwidth remains roughly the same even the corner frequency ω_c is reduced. The resonance amplitude, however, shows appreciable reduction.

Figure 6 compares the FRF when the span *d* is 6 mm. In Fig. 6, the thick solid line represents the FRF from the low resistance. According to Table 1, $\omega_c >> \omega_n$; therefore, the FRF starts with a constant magnitude and is followed by a resonance peak at ω_n. The 3-dB bandwidth is roughly 23.716 kHz. In contrast, the thin solid line in Fig. 6 represents the FRF corresponding to the specimen with high resistance. According to Table 1, $\omega_c << \omega_n$. As a result, the FRF starts with a constant magnitude at low frequency, but the magnitude rapidly

decreases as the driving frequency increases. The 3-dB bandwidth is roughly 9.548 kHz. In other words, the bandwidth has reduced by 59.74% as a result of the high electrical resistance. Moreover, the resonance amplitude has a reduction of one order of magnitude. Figures 5 and 6 show that the minimum of ω_c and ω_n govern the bandwidth and resonance amplitude of the PZT thin-film actuators.

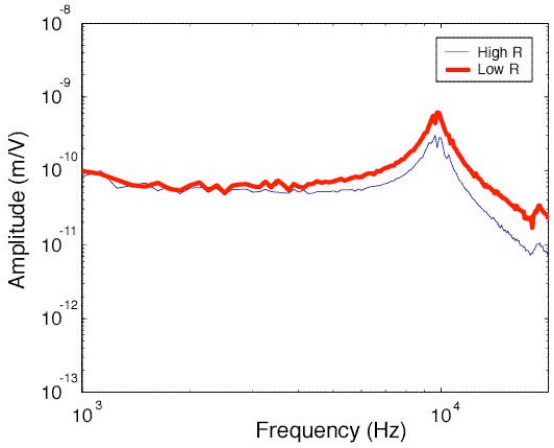

Figure 5. Frequency response functions for specimen with span d = 15 mm

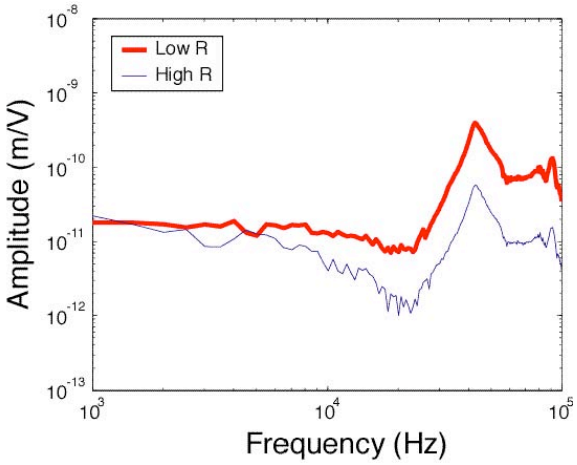

Figure 6. Frequency response functions for specimen with span d = 6 mm

CONCLUSIONS

Frequency response of PZT thin-film actuators primarily depends on two frequency parameters ω_n and ω_c, where ω_n is the lowest natural frequency of the actuator's mechanical structure and ω_c is the corner frequency of the electric *RC*-circuit of the actuator. The bandwidth of PZT thin-film actuators is limited by the smaller value of ω_n and ω_c. The resonance amplitude will be reduced when ω_c is less than ω_n. The amount of reduction depends on the difference in ω_c and ω_n.

REFERENCES

1. H. Kueppers, T. Leuerer, U. Schnakenberg, W. Mokwa, M. Hoffmann, T. Schneller, U. Boettger, R. Waser, PZT thin films for piezoelectric microactuator applications, *Sensors and ActuatorA*, 97-98 (2002) 690-684.
2. T. Shibata, K. Unno, E. Makino, and S. Shimada, Fabrication and characterization of diamond AFM probe integrated with PZT thin film sensor and actuator, *Sensors and Actuators A*, 114 (2004) 398-405.
3. A. M. Flynn, L. S. Tavrow, S. F. Bart, R. A. Brooks, D. J. Ehrlich, K. R. Udayakumar, and L. E. Cross, Piezoelectric micromotors for microrobots, *Journal of Microelectromechanical Systems*, 1 (1992) 44-51.
4. P. Muralt, M. Kohli, T. Maeder, A. Kholkin, K. Brooks, N. Setter, and R. Luthier, Fabrication and characterization of PZT thin-film vibrators for micromotors, *Sensors and Actuators A*, 48 (1995) 157-165.
5. P. Muralt, A. Kholkin, M. Kohli, and T. Maeder, Piezoelectric actuation of PZT thin-film diaphragms at static and resonant conditions, *Sensors and Actuators A*, 53 (1996) 398-404.
6. M. Dubois and P. Muralt, PZT thin film actuated elastic fin micromotor, *IEEE Transactions on Ultrasonics, Ferroelectrics, and Frequency Control*, 45 (1998) 1169-1177.
7. H. Goto, Two-dimensional micro optical scanner excited by PZT thin film microactuator, *Proceedings of SPIE Conference on Optoelectronic Materials and Devices*, Vol. 3419 (1998) 227-235.
8. A. Schroth, C. Lee, S. Matsumoto, and R. Maeda, Application of sol-gel deposited thin PZT film for actuation of 1D and 2D scanners, *Sensors and ActuatorsA*, 73 (1999) 1440152.
9. J. Tsaur, L. Zhang, R. Maeda, S. Matsumoto, and S. Khumpuang, Design and fabrication of 1D and 2D micro scanners actuated by double layered lead zirconate titanate (PZT) bimorph beams, *Jpn. J. Appl. Phys.*, 41 (2002) 4321-4326.
10. S. J. Gross, S. Tadigadapa, T. N. Jackson, S. Trolier-McKinstry, and Q. Q. Zhang, Lead-zirconate-titanate-based piezoelectric micromachined switch, *Applied Physics Letters*, 83 (2003) 174-176
11. Q. Q. Zhang, S. J. Gross, S. Tadigadapa, T. N. Jackson, F. T. Djuth, and S. Trolier-McKinstry, Lead zirconate titanate films for d_{33} mode cantilever actuators, *Sensors and Actuators A*, 105 (2003) 91-97.
12. F. F. C. Duval, R. A. Dorey, R. W. Wright, Z. Huang, and R. W. Whatmore, Fabrication and modeling of high-frequency PZT composite thick film membrane resonators, *IEEE Transactions on Ultrasonics, Ferroelectrics, and Frequency Control*, 51 (2004) 1255-1261.
13. H. Kuwajima and K. Matsuoka, Thin-film piezoelectric DSA for HDD, 38 (2002) 2186-2188.
14. N. Tagawa, K. Kitamura, and A. Mori, Design and fabrication of MEMS-based active slider using double-layered composite PZT thin film in hard disk drives, *IEEE Transactions on Magnetics*, 39 (2003) 926-931.

15. K. Suzuki, R. Maeda, J. Chu, T. Kato, and M. Kurita, An active head slider using a piezoelectric cantilever for in-situ flying-height control, *IEEE Trans Magn*, 39 (2003) 826-831.
16. P. Krulevitch, A. P. Lee, P. B. Ramsey, J. C. Trevino, J. Hamilton, and M. A. Northrup, Thin film shape memory alloy microactuators, *J Microelectromech*, 5 (1996) 270-282.
17. Hsu, Y. C., Wu, C. C., Lee, C. C., Cao, G. Z., and Shen I. Y., 2004, "Demonstration and Characterization of PZT Thin-Film Sensors and Actuators for Meso- and Micro-Structures," *Sensors and Actuators A—Physical*, Vol. 116, No. 3, pp. 367-377.